Toolbox

Editor's Note: Toolboxes are intended to briefly highlight a new method or a resource of general use in neuroscience or to critically analyze existing approaches or methods. For more information, see http://www.jneurosci.org/misc/itoa.shtml.

Quantification of Amyloid Precursor Protein and Tau for the Study of Axonal Traffic Pathways

Claire Goldsbury,[1,2] Edda Thies,[1] Sven Konzack,[1] and Eva-Maria Mandelkow[1]

[1]Max Planck Unit for Structural Molecular Biology, 22607 Hamburg, Germany, and [2]Brain and Mind Research Institute, University of Sydney, Camperdown, New South Wales 2050, Australia

We describe a procedure for quantifying the numbers of expressed fluorescent fusion proteins on vesicles transported in axons. The method can be used to estimate numbers of vesicle-anchored molecules moving in both anterograde and retrograde directions and is also applicable to cytosolic proteins. This is demonstrated using neurons (explanted retinal ganglion cells) transfected with yellow fluorescent protein-tagged amyloid precursor protein (APP–YFP) or cyan fluorescent protein–tau (CFP–tau). To calibrate the APP–YFP concentration on vesicles, standard solutions of recombinant YFP were imaged by confocal microscopy. For comparison, rotavirus-like particles containing a known number of 120 green fluorescent protein (GFP) molecules were imaged against standard solutions of GFP. On the basis of the calibration, the anterogradely and retrogradely moving APP vesicles contained 235 ± 145 and 218 ± 106 molecules, corresponding to mean fluxes of ~2000 anterograde and 700 retrograde APP–YFP molecules per minute per axon. Using recombinant CFP standard solutions for calibration, exogenous CFP–tau concentrations depended on the levels of expression but were typically 3–6 μM. The value of this procedure is that it is of general use in cell biology, in which knowing the numbers of membrane-anchored molecules is desirable. For example, the amount of APP transported into axonal versus dendritic compartments is relevant to the physiological function of APP and pathological events in Alzheimer's disease.

Introduction

Cleavage of the amyloid precursor protein (APP) and generation of amyloid-β (Aβ) peptides is central to the pathology of Alzheimer's disease (AD) (Haass, 2004). This occurs in conjunction with phosphorylation, somatodendritic accumulation, and aggregation of the microtubule-binding protein tau that is normally localized in the axon (Garcia and Cleveland, 2001). We have shown that elevated tau can inhibit the transport of APP vesicles and organelles out of the cell body and into axons (Stamer et al., 2002). This is of potential importance for AD in which loss of synapses is the major correlate of disease progression (Terry, 2006). It is therefore important to understand the spatial distribution of APP cleavage in polarized neurons both under normal circumstances and under pathological conditions in which changes in tau localization and phosphorylation occur.

It has been proposed that Aβ is generated in both dendrites and axons (Morin et al., 1993; Amaratunga and Fine, 1995; De Strooper et al., 1995; Buxbaum et al., 1998; Lazarov et al., 2002; Sheng et al., 2002; Abad-Rodriguez et al., 2003; Takahashi et al., 2004; Lee et al., 2005; Almeida et al., 2006; Rajendran et al., 2006). However, the relative probability of cleavage events in these compartments is not known. Temporal quantification of the number of APP molecules moving through axons and arriving at neurite tips would assist in determining this (Morin et al., 1993). Such estimations could theoretically be linked to biochemical measurements of Aβ concentrations and allow the relative frequency of cleavage in dendrites versus axons to be evaluated. Toward this goal, we have quantified the number of APP molecules moving through explanted retinal ganglion cell (RGC) axons per minute in both the anterograde direction toward the growth cone tip and in the retrograde direction back toward the cell body.

Fluorescent fusion proteins of green fluorescent protein (GFP) and its cyan (CFP) and yellow (YFP) derivatives are widely used for live-cell imaging. Such constructs have revealed diverse information about the subcellular localization, dynamics, and trafficking of membrane, cytoskeletal, and other proteins (Wacker et al., 1997; Kaether et al., 2000, 2006; Ackermann and Matus, 2003; Ebihara et al., 2003; Mandelkow et al., 2004; Wittmann and Waterman-Storer, 2005; Ward and Lippincott-Schwartz, 2006). Recently, quantitative methods have been applied to pin down fluorescent molecules and their complexes involved in cellular

Received Nov. 20, 2006; revised Feb. 14, 2007; accepted Feb. 15, 2007.

This work was supported in part by the Deutsche Forschungsgemeinschaft. We thank S. Hübschmann, A. Grabbe, and M. Bilang for excellent technical assistance and Drs. A. Marx, J. Biernat, and E. Mandelkow for stimulating discussions. We also thank A. Charpilienne (Virologie Moleculaire et Cellullaire, Centre National de la Recherche Scientifique–Institut National de la Recherche Agronomique, Cedex, France) for kindly providing the GFP-tagged rotavirus.

Correspondence should be addressed to Dr. Claire Goldsbury, Brain and Mind Research Institute, University of Sydney, 100 Mallett Street, Camperdown, New South Wales 2050, Australia. E-mail: cgoldsbury@usyd.edu.au.

DOI:10.1523/JNEUROSCI.5024-06.2007

 0270-6474/07/273357-07$15.00/0

events (Fink et al., 1998; Charpilienne et al., 2001; Rabut et al., 2004; Sugiyama et al., 2005). We use recombinant YFP and CFP solutions as calibration standards for estimating the numbers of APP–YFP molecules on individual APP vesicles and axonal concentrations of transfected CFP-tagged tau protein. The flux per minute of APP–YFP molecules moving along axons and arriving at the growth cone could be calculated. These data will aid ongoing efforts to determine differences in axonal versus somatodendritic APP cleavage that are relevant to the physiological function of APP and pathological events in AD. Additionally, quantification of intracellular tau concentrations will support experiments aimed at understanding the role of tau in transport inhibition, microtubule dynamics, phosphorylation, and aggregation in AD.

Materials and Methods

Construction of bacterial vectors for expression of CFP and YFP. CFP and YFP sequences were amplified from the pECFP-C1 and pEYFP-C1 vectors (Clontech, Heidelberg, Germany), respectively, using the following primers: 5′-CCATATGGTGAGCAAGGGCGAGGAGCTGTT-3′; 5′-GGGATCCTTACTTGTACAGCTCGTCCATGCCGAGAGTGA-3′.

Unique *Nde*I and *Bam*HI restriction sites were thus introduced during PCR amplification. The PCR product was introduced into the pCR-TOPO blunt vector (Invitrogen, Karlsruhe, Germany) for sequencing. The *Nde*I–*Bam*HI fragment was then excised, purified from agarose gel, and ligated with the *Nde*I–*Bam*HI-digested and -purified pET-16b vector (Novagen, Darmstadt, Germany). Ligation was performed using the Quick Ligation kit (New England Biolabs, Beverly, MA) according to the manufacturer's instructions. After transformation in XL2 blue Ultracompetent cells (Stratagene, La Jolla, CA), clones were analyzed by restriction digestion with *Nde*I and *Bam*HI. The pET16-b plasmids containing the resulting CFP or YFP insert were then transformed into BL21(DE3) bacteria (Stratagene) for protein expression.

Recombinant CFP, YFP, and GFP. Transformed BL21/DE3 bacteria were grown until OD >0.6, and recombinant protein expression was induced for 3 h by the addition of 0.4 mM isopropyl β-D-1-thiogalactopyranoside to the medium. Cells were then harvested and lysed in 50 mM Tris-HCl, pH 7.2, containing 1 mM $MgS0_4$, 50 mM NaCl, 1 mM β-mercaptoethanol, and protease inhibitors. A French Press was used for the lysis. Lysates were cleared by centrifugation (70,000 × *g* for 1 h at 4°C). Cleared lysates were applied to high-trap nickel affinity chromatography columns (GE Healthcare, Munich, Germany) and the His-tagged protein eluted with an imidazole gradient. Fractions were concentrated, and the protein was exchanged into 10 mM Tris/10 mM EDTA by dialysis. The protein concentration of the final stock solutions were determined by Coomassie staining on SDS-PAGE gels alongside known BSA standards and by peptide bond absorbance at 214 nm calibrated with BSA standards. Standard GFP solutions were purchased from Clontech (Mountain View, CA).

Preparation and transfection of chick retina explants. Retina explants were prepared from White Leghorn chicks at embryonic day 6 as described previously (Walter et al., 1987). The dissected retina was attached to nitrocellulose filters, cut into ~2-mm-wide strips, and mounted with the ganglion cell layer face down onto glass-bottomed dishes that had been coated overnight with 4 μg/ml laminin (Sigma-Aldrich, Munich, Germany). Explants were maintained in DMEM/F-12 (Invitrogen) containing 10% FCS, 0.4% methyl cellulose (Sigma-Aldrich), and antibiotics (penicillin and streptomycin; Invitrogen). After 1 d, to allow ganglion cell axonal outgrowth, the explants were transfected with APP–YFP constructs or CFP–tau (htau40, the longest isoform in the human CNS; 441 residues) using recombinant adenoviral vectors generated as described previously (Stamer et al., 2002; Goldsbury et al., 2006). The Swedish mutant of APP695 (K670N/M671L) was used because this variant produces readily detectable Aβ peptides when transfected in retina explant cultures (Goldsbury et al., 2006). Selected pShuttleCMV plasmids were kindly provided by Dr. B. Vogelstein (Johns Hopkins University, Baltimore, MD) (He et al., 1998). Adenoviruses were amplified in mammalian cells (e.g., HEK 293; Microbix Biosystems, Toronto, Ontario, Canada), and resulting viral suspensions were purified by CsCl gradient centrifugations (Kanegae et al., 1994).

Confocal microscopy and calculation of the number of APP–YFP molecules per vesicle. Transfected RGC axons, GFP-tagged rotavirus-like particles (Charpilienne et al., 2001), and standard recombinant protein solutions were imaged with an LSM 510 confocal microscope (Zeiss, Jena, Germany) equipped with a 63× oil-immersion objective and a 37°C air-heated object plane. The argon laser lines at 458, 514, and 488 nm with appropriate emission filters were used for excitation and detection of CFP, YFP, and GFP, respectively. While imaging APP–YFP-transfected axons or GFP-tagged rotavirus-like particles, conditions were established in which the fluorescent signal was not saturated and the signal-to-noise ratio was optimal. All imaging parameters [laser energy (10–20% power), gains, offset, and pinhole diameter (either 1.0 or 1.5 Airy units (AU)] were then kept constant during imaging. Time-lapse series of APP–YFP vesicles moving through axons were made. Typically, 50–100 frames were captured at intervals of 0.5–1.5 s. For this, a slice was chosen close to the glass surface where the vesicles moving into the axon were in focus. Identical imaging conditions were subsequently used to scan droplets of serially diluted recombinant protein solutions of known concentrations. These solutions were used to create standard curves of micromolar YFP, CFP, or GFP versus mean pixel intensity after background subtraction [relative intensity units (RIU)]. Protein solutions were diluted in 10 mM Tris-HCl/10 mM EDTA, pH 7.9, and applied to dry glass coverslips (#1; Menzel-Glaser, Braunschweig, Germany) precoated with 10 mg/ml BSA. The RIU increased linearly with the micromolar recombinant fluorescent protein concentration. No hardware pinhole adjustments were made between imaging the axons or rotavirus particles and standard protein solutions.

Using the Zeiss LSM software, each APP–YFP vesicle or rotavirus-like particle was traced and enclosed in a region of interest, and the region was then copied using the "extract region" function. The vesicle was selected only in the frame of its first appearance in the axon. Because of bleaching, subsequent images of the vesicle in following frames were not used. A histogram was then displayed that showed the intensity distribution of the pixels within the vesicle or rotavirus-like particle. The mean pixel intensity after background subtraction was typically 30–80 RIU for APP–YFP vesicles. The mean apparent concentration *C* (micromolars) in the region of interest was then extrapolated from a standard recombinant fluorescent protein curve generated as described above using the same imaging conditions as those used to image the vesicles or rotavirus-like particles. Under the conditions used to image the RGC axons and standard curves, the pinhole was set to either 1 or 1.5 AU, corresponding to a slice thickness, *z*, of ~0.8 or 1.2 μm (separate YFP standard curves were generated for the two different pinhole diameters). The estimations of *z* were checked using Equations 1 and 2 below (Wilhelm et al., 2003):

$$z \approx \mathrm{FWHM}_{\mathrm{det,axial}} = \sqrt{\left(\frac{0.88 \times \lambda_{\mathrm{em}}}{n - \sqrt{n^2 - \mathrm{NA}^2}}\right)^2 + \left(\frac{\sqrt{2} \times n \times \mathrm{PH}}{\mathrm{NA}}\right)^2}, \quad (1)$$

where

$$\mathrm{PH} = \mathrm{AU} \frac{\times 1.22 \times \lambda_{\mathrm{ex}}}{\mathrm{NA}}, \quad (2)$$

where $\mathrm{FWHM}_{\mathrm{det,axial}}$ is the full-width at half-maximum, detection beam, and axial direction, an approximation of the slice thickness *z*; λ_{em} is the emission wavelength (525 nm for YFP or 509 nm for GFP); λ_{ex} is the wavelength of illuminating laser light (514 nm for YFP or 488 nm for GFP); *n* is the refractive index of immersion liquid (1.52); and NA is the numerical aperture of the objective (1.4).

The area *A* through which the fluorescence is spread (pixel size in square micrometers times the number of pixels enclosing the vesicle) was typically in the range of 0.2–3.5 μm^2. The apparent volume *V* (cubed micrometers) of the vesicle was determined by multiplying the slice thickness, *z*, by *A*. Finally, the number of mol-

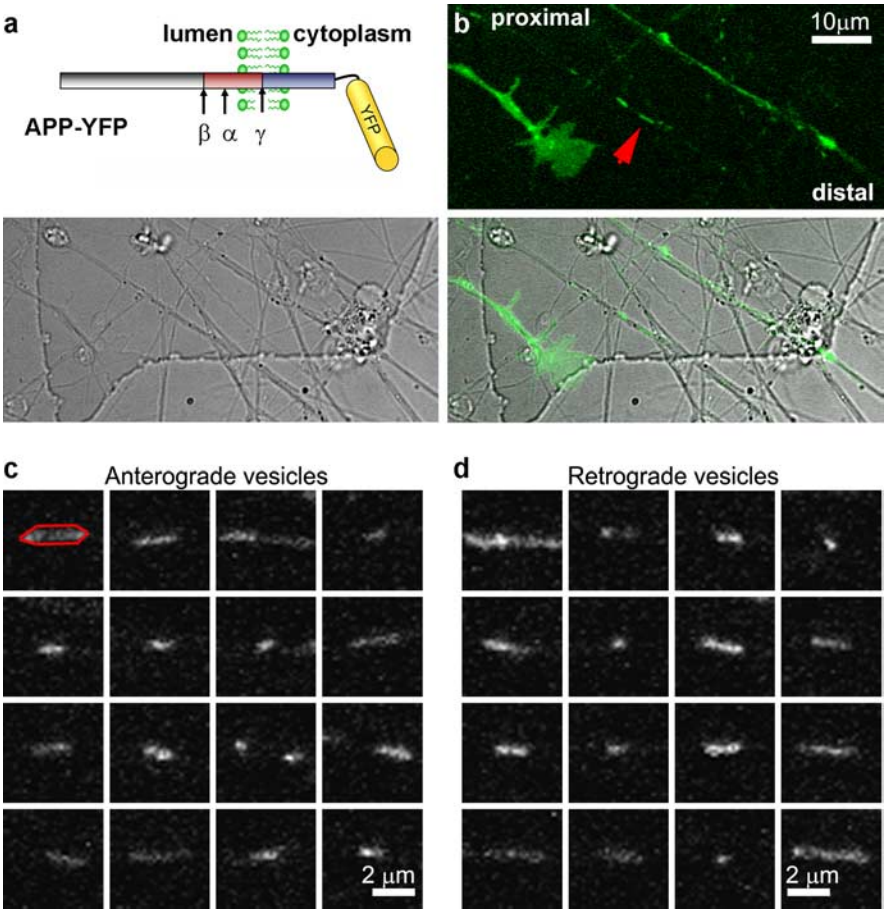

Figure 1. Time-lapse confocal microscopy of YFP-tagged APP vesicles in RGC axons. ***a***, Scheme of the APP–YFP construct (Swedish mutant of APP) used in these experiments. The YFP tag is on the C terminus and is therefore outside the vesicle. Cleavage sites for α-, β-, and γ-secretases are indicated. The Aβ fragment is shaded in red. ***b***, In RGC axons, vesicles move by fast axonal transport predominantly in the anterograde direction (proximal to distal). In this still frame from a time-lapse series, many axons can be seen (top, fluorescence signal in green; bottom, phase image and its overlay with the fluorescence), only a few of which are transfected (green). A transfected growth cone can be seen to the left of the frame as well as vesicles (arrow). ***c***, ***d***, Vesicles were defined as they moved in to the distal (retrograde) or proximal (anterograde) end of the axon using the region-of-interest tool in the microscope software (red shape). The galleries of anterograde (***c***) and retrograde (***d***) vesicles illustrate their range of sizes and fluorescence intensities.

ecules N in each vesicle was calculated by multiplying the extrapolated mean apparent C by V, Avogadro's number (6.023×10^{23}), and a conversion factor, $f = 10^{-21}$ (converting micromolars and cubed micrometers to M and L):

$$N = C\,[\mu\mathrm{M}] \times V\,[\mu\mathrm{m}^3] \times 6.023 \times 10^{23} \times f. \quad (3)$$

Measurements of vesicle fluxes were made from movies of individual axons viewed in the LSM Image Browser (Zeiss). This was done by counting the number of new vesicles appearing and moving processively in each direction per minute over the period of imaging (typically, the axon was imaged at intervals of 0.5–1.5 s for 1–2 min). The mean per minute flux was calculated by averaging the counts determined from several axons selected from different retina preparations (Goldsbury et al., 2006).

Results

Transport of APP–YFP molecules in vesicles of RGC axons

Ganglion cell axons readily grow out from explanted chick retina and provide a useful model system for investigating axonal transport (Walter et al., 1987; Stamer et al., 2002). When APP–YFP (Fig. 1*a*) is expressed in these axons, it moves in vesicular and tubular packages via kinesin-mediated fast axonal transport (Stamer et al., 2002), similar to its behavior in primary hippocampal neurons (Kaether et al., 2000). The directionality (anterograde vs retrograde) characteristics of the vesicles can be clearly defined. Furthermore, because the explants secrete Aβ (Goldsbury et al., 2006), they provide a useful model system for investigating effects on APP processing (e.g., the linkage between axonal transport and Aβ generation). Such questions require quantitative determinations of the number of APP molecules transported versus the number of Aβ molecules generated. We therefore estimated the number of APP–YFP molecules typically existing in individual transport packages moving along RGC axons. From the flux rates of vesicles per minute moving through the axons, we then extrapolated the number of APP–YFP molecules per minute that must arrive at the growth cones at the end of the axon. RGCs were transfected with APP–YFP using adenovirus and were imaged by time-lapse confocal microscopy (Fig. 1*b*). APP–YFP vesicles moving in the anterograde (Fig. 1*c*) and retrograde (Fig. 1*d*) directions were selected using the region-of-interest tool in the Zeiss LSM software. To avoid loss of signal as a result of bleaching from repeated imaging, the regions of interest were defined at the time point when the vesicle first appeared in the axon.

Imaging standard solutions of recombinant YFP and CFP

To estimate the concentration of APP–YFP on selected vesicles, or the CFP–tau concentration in the axonal cytoplasm (see below), we generated recombinant YFP and CFP. The concentrations of the recombinant protein solutions were determined by Coomassie staining after SDS-PAGE and additionally by peptide bond absorbance at 214 nm (Fig. 2*a*). The solutions were serially diluted, and droplets were placed on BSA-coated coverslips (Fig. 2*b*). The BSA was used to prevent YFP from strongly adsorbing to the glass surface and distorting the measurements (Fig. 2*c*). Confocal stacks slicing through the droplets were made using identical imaging settings to as used for APP–YFP vesicles (Figs. 2, 3) or CFP–tau (see Fig. 5). On BSA-coated glass, the intensity in the YFP droplets fluctuated slightly as the slice moved from ~1 to ~20 μm above the glass surface (Fig. 2*c*), but the mean pixel intensity versus concentration was linear within this distance (Fig. 2*d*).

Quantification of the number of APP–YFP molecules in transport vesicles

Using YFP standard curves, the mean pixel intensities in the selected APP vesicles (Fig. 3*a*) were extrapolated to mean apparent YFP concentrations. The volume containing the fluorescence from the entire vesicle was calculated by multiplying the area of the region of interest by the slice thickness. Typical volumes ranged

from 0.5 to 3.7 μm^3 (mean, 1.6 μm^3) (note that the real volume of the vesicle is, of course, much smaller than this apparent volume seen by light microscopy, but the region-of-interest tool allows the entire area through which the fluorescence is spread to be captured). This was then used to calculate the total number of YFP molecules from the mean apparent YFP concentration. Calculated in this way, the number of APP–YFP molecules in the vesicles ranged from <100 up to a maximum of ~800. Vesicles containing the full range of molecules were detected in single axons. The distribution obtained from anterograde and retrograde moving vesicles is displayed in the histogram in Figure 3*b*. It shows that, on average, anterograde moving vesicles contained 235 ± 145 molecules ($n = 39$) and retrograde moving vesicles contained 218 ± 106 molecules ($n = 27$) (mean ± SD; note that these values are dependent on transfection and do not represent the endogenous concentrations of APP in native vesicles). Interestingly, anterograde and retrograde moving vesicles contained a similar distribution of number of molecules. The mean flux rate in these axons was 8.4 ± 2.4 anterograde and 3.0 ± 1.2 retrograde vesicles per minute (mean ± SEM) (Goldsbury et al., 2006). Taking the mean number of molecules per vesicle, this would correspond to mean fluxes of 1974 anterograde and 654 retrograde molecules per minute per axon.

Verification of the quantification method

To verify the method for estimating the number of APP–YFP molecules in individual APP–YFP vesicles, we imaged GFP-tagged rotavirus-like particles against standard solutions of recombinant GFP (Fig. 4). Previous estimates using electron microscopy combined with gel electrophoresis showed that these particles contain 120 molecules of GFP (Charpilienne et al., 2001). Our estimates using a GFP standard solution imaged by confocal microscopy revealed 156 ± 54 GFP molecules per rotavirus-like particle (mean ± SD; $n = 22$), in good agreement with the previous measurement by Charpilienne et al. (2001). Examples of particles used to make these measurements are indicated by white circles in Figure 4*a*. It can be seen in Figure 4*a* that there were some very bright spots that potentially represented aggregated or multiple adjacent rotavirus-like particles (arrow). These bright spots were therefore not included in our measurements.

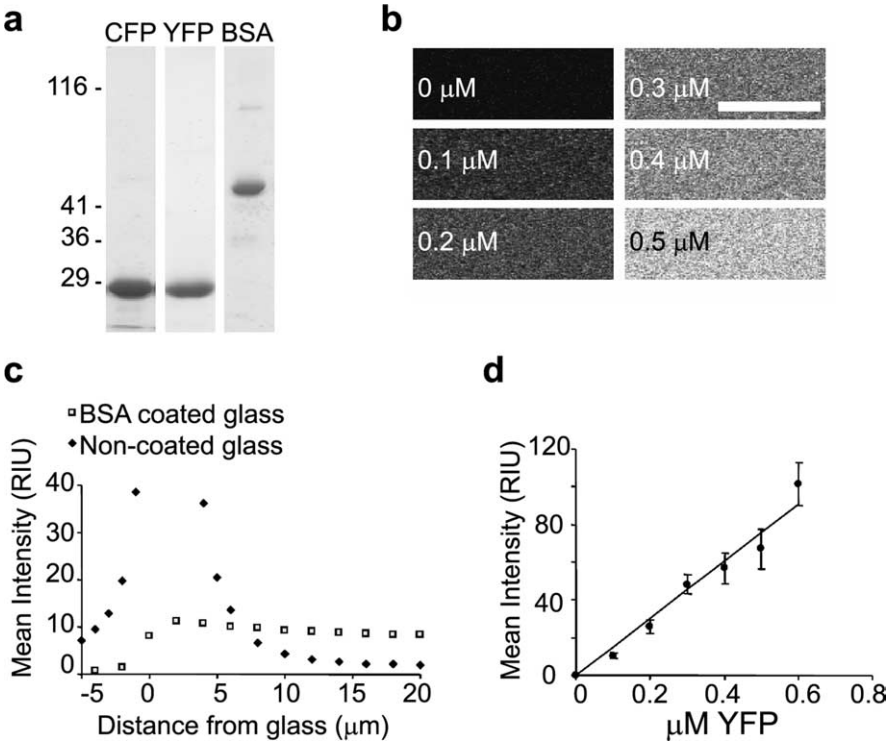

Figure 2. Confocal imaging of standard solutions of recombinant YFP. ***a***, Purified recombinant proteins were loaded on 10% SDS-PAGE gels alongside increasing amounts of known BSA standards. The Coomassie-stained band intensity was then used to determine the concentration of the recombinant protein relative to the BSA standards (one shown). The fluorescent protein concentration was also estimated using peptide bond absorbance at 214 nm (not shown). ***b***, Droplets of recombinant YFP on BSA-coated glass coverslips imaged by confocal microscopy. Confocal images <20 μm from the glass surface were made for YFP solutions at increasing micromolar concentrations as indicated. Scale bar, 10 μm. ***c***, BSA coating shields the glass surface from adsorption of YFP molecules, creating a more uniform YFP concentration in the bulk solution. Without BSA, YFP protein strongly adsorbed to the surface causing peak intensity close to the glass and a sharp tapering off of intensity further from the glass. Because of optical effects, even with BSA coating, the intensities slightly decreased as the confocal slice was moved further away from the glass. Therefore, intensity measurements were restricted to slices between 1 and 20 μm from the glass surface. ***D***, A typical calibration curve: mean pixel intensity (RIU) versus YFP concentration.

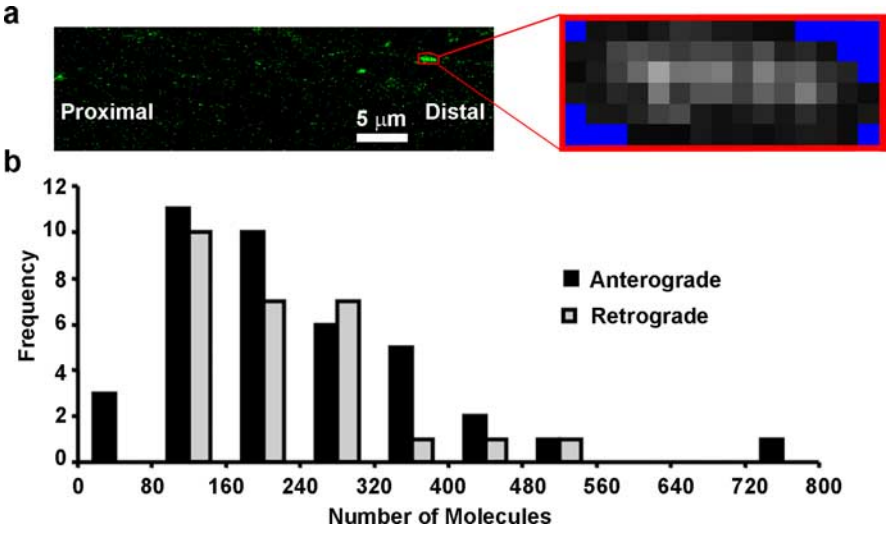

Figure 3. The distribution of the number of APP–YFP molecules per vesicle. ***a***, Vesicles were selected as they moved into the axon. A still frame from a time-lapse series is shown. An example of a selected vesicle used to determine the mean pixel intensity is illustrated (inset). The blue color is outside of the region of interest. The mean pixel intensity was used to calculate the number of YFP molecules in the vesicle (see Materials and Methods). ***b***. Data collected from many vesicles and displayed in a histogram illustrates that anterograde and retrograde vesicles contained similar numbers of molecules: 235 ± 145 and 218 ± 106 molecules (mean ± SD; $n = 39$ and $n = 27$), respectively. The vesicles contained a range of molecules, from ~60 up to 800, as reflected in the broad distribution of the histogram.

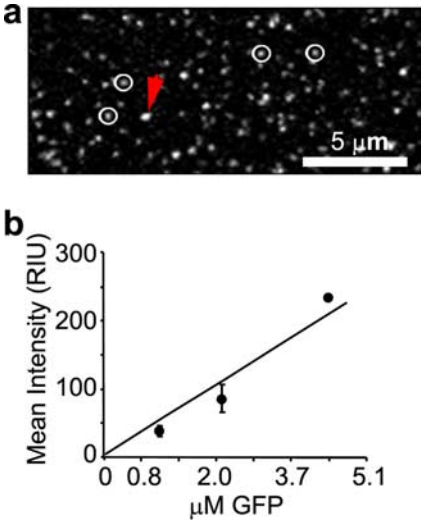

Figure 4. Imaging of GFP-tagged rotavirus-like particles by confocal microscopy. ***a***, Rotavirus-like particles were imaged by confocal microscopy, defined using the region-of-interest tool of the software (white circles), and their mean pixel intensities were determined. ***b***, A calibration curve of mean pixel intensity versus GFP concentration was created using droplets of GFP solutions of increasing concentrations imaged on BSA-coated coverslips under identical conditions to the virus particles. Using this curve, the mean number of GFP molecules per virus particle was calculated to be 156 ± 54 (mean ± SD; $n = 22$) (see Results). The arrow in ***a*** indicates a bright spot probably representative of multiple particles. Such potential aggregates were excluded from the measurements.

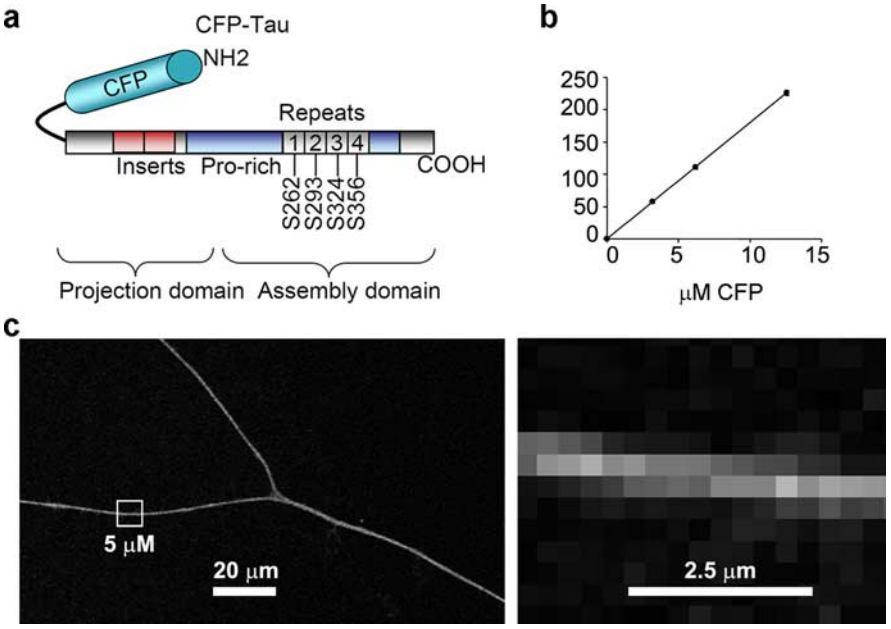

Figure 5. Estimation of the intra-axonal CFP–tau concentration by confocal imaging of standard solutions of recombinant CFP. ***a***, Scheme of the CFP–tau construct (full-length, wild-type, 4-repeat tau) used in these experiments. The CFP tag is on the N terminus (NH2). COOH, C terminus. ***b***, Droplets of recombinant CFP solutions of increasing concentrations were imaged on BSA-coated coverslips by confocal microscopy, resulting in a linear calibration curve of mean pixel intensity versus concentration. ***c***, In RGC axons expressing CFP–tau, the CFP concentration was estimated from the mean intensity in a region of interest. The image on the right shows a magnification of the region of interest boxed on the left that contains an estimated CFP–tau concentration of 5 μM. Note that the optical slice thickness z (<0.8 μm) means that axons of ~ 1 μm in diameter would be larger than the imaged volume.

Axonal concentration of overexpressed CFP–tau estimated by imaging standard solutions of recombinant CFP

A similar approach was used to estimate the concentration of CFP–tau (Fig. 5*a*) in transfected RGC axons. Droplets of serially diluted CFP standard solution were prepared and imaged on BSA-coated coverslips as described above for YFP. The resulting intensity versus concentration calibration curve yielded a linear relationship (Fig. 5*b*). Axons transfected with CFP–tau were imaged under identical conditions as the calibration solutions (Fig. 5*c*). The mean pixel intensities in regions of interest in the axon were then extrapolated to a mean CFP concentration by reading off the calibration curve. The concentration of CFP–tau varied with different levels of expression but was typically in the range of 3–6 μM.

Discussion

Transport and cleavage of APP in neurons generates C-terminal fragments (CTFs) and potentially toxic Aβ peptides central to the neuropathology of AD. Temporal spatial quantification of APP transport and cleavage is important for dissecting physiological roles (Turner et al., 2003; Muresan and Muresan, 2005; Priller et al., 2006; Satpute-Krishnan et al., 2006) and toxic effects (Walsh et al., 2002). As a basis to extend this understanding, we set out to quantify the throughput of APP molecules moving in axons by fast anterograde transport. The other protein of major importance in AD is the microtubule-associated protein tau, which stabilizes axonal microtubules and controls their dynamics. Tau transport (Mercken et al., 1995) is much slower than that of APP (Buxbaum et al., 1998; Kaether et al., 2000), but nevertheless, "slow axonal transport" could still be mediated by molecular motors such as kinesin (Baas and Buster, 2004). Overexpression of tau in neurons compromises the transport machinery by interfering with the proper function of kinesin (Trinczek et al., 1999; Stamer et al., 2002). Therefore, in studies addressing this relationship, it is important to know in absolute terms what the local concentration of tau is and how it develops with time. For these reasons, we also developed a method to quantify the axonal concentration of exogenously expressed tau. Although we investigated APP–YFP and CFP–tau, these procedures would be applicable for quantifying any vesicle-anchored or cytosolic-expressed fluorescent protein.

These issues were approached by generating recombinant YFP and CFP standard solutions to calibrate the fluorescence derived from transfected APP–YFP and CFP–tau inside RGC axons imaged by live-cell confocal microscopy. RGC axons were chosen for these experiments because of their well defined polarity allowing unambiguous distinction of forward and reverse transport as well as relatively little background fluorescence. Dendritic processes exhibit potentially increased complexity because of a less well defined polarity and background fluorescence from ongoing protein synthesis. Time-lapse images of transfected RGCs showed APP–YFP vesicles moving through axons in both anterograde and retrograde directions. Using identical microscope settings, a dilution series of the YFP standard solution was also imaged, and a calibration curve of mean pixel intensity versus YFP concentration produced. This enabled the apparent APP–YFP concentration in individual vesicles to be extrapolated. The number of APP–YFP molecules was then calculated by multiplying by the volume enclosing the fluorescence of the vesicle. The same approach was used to estimate intra-axonal CFP–tau concentrations. From knowing the mean flux rate of APP–YFP vesicles per minute in the antero-

grade and retrograde directions (8.4 and 3.0 vesicles per minute, respectively) (Goldsbury et al., 2006), it follows that the number of molecules per minute could be calculated from the mean number of molecules per vesicle as determined above. Using this approach, we estimated the detectable anterograde and retrograde moving vesicles contained 235 ± 145 and 218 ± 106 molecules, respectively (mean ± SD), corresponding to mean fluxes of ~2000 anterograde and 700 retrograde APP–YFP molecules per minute per axon. In addition to full-length APP, CTFs are also transported anterogradely and accumulate at nerve terminals (Amaratunga and Fine, 1995; Buxbaum et al., 1998). APP–YFP CTFs could therefore account for some of the vesicle fluorescence and be included in the calculated numbers of molecules. Interestingly, we did not find a difference in the fluorescence intensities or sizes of anterograde versus retrograde moving vesicles and speculate that at least some of the retrograde packages could be outbound vesicles that have changed direction. Alternatively, they may be endocytosed vesicles containing full-length APP and CTFs (Yamazaki et al., 1995). The exogenous tau concentration in axons transfected with CFP–tau depended on the level of expression but was typically 3–6 μM.

Additional experiments, aided by the quantification of axonally transported APP presented here, could potentially be used to determine the relative contributions of axons and dendrites to the generation of Aβ secreted into the cell medium. Pure primary neuronal cultures of RGCs or CNS neurons would be suitable for such correlations. Importantly, the transport properties of APP vesicles in CNS dispersion cultures appears to be, more or less, identical to explanted RGCs (Kaether et al., 2000; Stamer et al., 2002; Goldsbury et al., 2006).

The method used to determine the number of fluorescent molecules in single vesicles was checked by imaging rotavirus-like particles containing a known number of 120 GFP molecules (Charpilienne et al., 2001). Using standard GFP solutions, we estimated 156 ± 54 GFP molecules per particle. This indicates that our method produces estimates within the correct order of magnitude. Other factors that could affect the data include chromaphore formation efficiency in RGCs compared with in recombinant protein solutions. Sugiyama et al. (2005) recently estimated the chromaphore efficiency of recombinant GFP and YFP to be 91% compared with 60–90% for transfected GFP and YFP fusion proteins expressed in primary neurons. Therefore, our estimates of transfected APP–YFP molecules could be slightly on the low side because some of the YFP chromaphores may not be active when fused to APP. Also affecting the estimation is the error involved in determining the volume through which the fluorescence of the vesicle is spread. For example, the estimation of the slice thickness is approximated by the FWHM. Also, any fluorescence lost above and below the field of the optical slice would not have been included in the calculations. Taking together these deficiencies, the estimation of the number of APP–YFP molecules per vesicle would not be affected by more than a factor of ~2. Bearing this in mind, our data form a basis for additional work, including measurements aimed at increasing understanding of the spatial distribution of APP cleavage and Aβ generation in normal neurons as well as those affected by AD.

References

Abad-Rodriguez J, Ledesma MD, Craessaerts K, Perga S, Medina M, Delacourte A, Dingwall C, De Strooper B, Dotti CG (2003) Neuronal membrane cholesterol loss enhances amyloid peptide generation. J Cell Biol 167:953–960.

Ackermann M, Matus A (2003) Activity-induced targeting of profilin and stabilization of dendritic spine morphology. Nat Neurosci 6:1194–1200.

Almeida CG, Takahashi RH, Gouras GK (2006) β-Amyloid accumulation impairs multivesicular body sorting by inhibiting the ubiquitin-proteasome system. J Neurosci 26:4277–4288.

Amaratunga A, Fine RE (1995) Generation of amyloidogenic C-terminal fragments during rapid axonal transport in vivo of beta-amyloid precursor protein in the optic nerve. J Biol Chem 270:17268–17272.

Baas PW, Buster DW (2004) Slow axonal transport and the genesis of neuronal morphology. J Neurobiol 58:3–17.

Buxbaum JD, Thinakaran G, Koliatsos V, O'Callahan J, Slunt HH, Price DL, Sisodia SS (1998) Alzheimer amyloid protein precursor in the rat hippocampus: transport and processing through the perforant path. J Neurosci 18:9629–9637.

Charpilienne A, Nejmeddine M, Berois M, Parez N, Neumann E, Hewat E, Trugnan G, Cohen J (2001) Individual rotavirus-like particles containing 120 molecules of fluorescent protein are visible in living cells. J Biol Chem 276:29361–29367.

De Strooper B, Simons M, Multhaup G, Van Leuven F, Beyreuther K, Dotti CG (1995) Production of intracellular amyloid-containing fragments in hippocampal neurons expressing human amyloid precursor protein and protection against amyloidogenesis by subtle amino acid substitutions in the rodent sequence. EMBO J 14:4932–4938.

Ebihara T, Kawabata I, Usui S, Sobue K, Okabe S (2003) Synchronized formation and remodeling of postsynaptic densities: long-term visualization of hippocampal neurons expressing postsynaptic density proteins tagged with green fluorescent protein. J Neurosci 23:2170–2181.

Fink C, Morgan F, Loew LM (1998) Intracellular fluorescent probe concentrations by confocal microscopy. Biophys J 75:1648–1658.

Garcia ML, Cleveland DW (2001) Going new places using an old MAP. Tau, microtubules and human neurodegenerative disease. Curr Opin Cell Biol 13:41–48.

Goldsbury C, Mocanu MM, Thies E, Kaether C, Haass C, Keller P, Biernat J, Mandelkow E, Mandelkow E-M (2006) Inhibition of APP trafficking by tau protein does not increase the generation of amyloid-β peptides. Traffic 7:873–888.

Haass C (2004) Take five—BACE and the gamma-secretase quartet conduct Alzheimer's amyloid beta-peptide generation. EMBO J 23:483–488.

He TC, Zhou S, da Costa LT, Yu J, Kinzler KW, Vogelstein B (1998) A simplified system for generating recombinant adenoviruses. Proc Natl Acad Sci USA 95:2509–2514.

Kaether C, Skehel P, Dotti CG (2000) Axonal membrane proteins are transported in distinct carriers: a two-color video microscopy study in cultured hippocampal neurons. Mol Biol Cell 11:1213–1224.

Kaether C, Schmitt S, Willem M, Haass C (2006) Amyloid precursor protein and Notch intracellular domains are generated after transport of their precursors to the cell surface. Traffic 7:408–415.

Kanegae Y, Makimura M, Saito I (1994) A simple and efficient method for purification of infectious recombinant adenovirus. Jpn J Med Sci Biol 47:157–166.

Lazarov O, Lee M, Peterson DA, Sisodia SS (2002) Evidence that synaptically released β-amyloid accumulates as extracellular deposits in the hippocampus of transgenic mice. J Neurosci 22:9785–9793.

Lee EB, Zhang B, Liu K, Greenbaum EA, Doms RW, Trojanowski JQ, Lee VM (2005) BACE overexpression alters the subcellular processing of APP and inhibits Abeta deposition in vivo. J Cell Biol 168:291–302.

Mandelkow E-M, Thies E, Trinczek B, Biernat B, Mandelkow E (2004) MARK/PAR1 kinase is a regulator of microtubule-dependent transport in axons. J Cell Biol 167:99–110.

Mercken M, Fischer I, Kosik KS, Nixon RA (1995) Three distinct axonal transport rates for tau, tubulin, and other microtubule-associated proteins: evidence for dynamic interactions of tau with microtubules *in vivo*. J Neurosci 15:8259–8267.

Morin PJ, Abraham CR, Amaratunga A, Johnson RJ, Huber G, Sandell JH, Fine RE (1993) Amyloid precursor protein is synthesized by retinal ganglion cells, rapidly transported to the optic nerve plasma membrane and nerve terminals and metabolized. J Neurochem 61:464–473.

Muresan Z, Muresan V (2005) Coordinated transport of phosphorylated amyloid-beta precursor protein and c-Jun NH2-terminal

kinase-interacting protein-1. J Cell Biol 171:615–625.
Priller C, Bauer T, Mitteregger G, Krebs B, Kretzschmar HA, Herms J (2006) Synapse formation and function is modulated by the amyloid precursor protein. J Neurosci 26:7212–7221.
Rabut G, Doye V, Ellenberg J (2004) Mapping the dynamic organization of the nuclear pore complex inside single living cells. Nat Cell Biol 6:1114–1121.
Rajendran L, Honsho M, Zahn TR, Keller P, Geiger KD, Verkade P, Simons K (2006) Alzheimer's disease beta-amyloid peptides are released in association with exosomes. Proc Natl Acad Sci USA 103:11172–11177.
Satpute-Krishnan P, DeGiorgis JA, Conley MP, Jang M, Bearer EL (2006) A peptide zipcode sufficient for anterograde transport within amyloid precursor protein. Proc Natl Acad Sci USA 103:16532–16537.
Sheng JG, Price DL, Koliatsos VE (2002) Disruption of corticocortical connections ameliorates amyloid burden in terminal fields in a transgenic model of Aβ amyloidosis. J Neurosci 22:9794–9799.
Stamer K, Vogel R, Thies E, Mandelkow E, Mandelkow EM (2002) Tau blocks traffic of organelles, neurofilaments, and APP vesicles in neurons and enhances oxidative stress. J Cell Biol 156:1051–1063.
Sugiyama Y, Kawabata I, Sobue K, Okabe S (2005) Determination of absolute protein numbers in single synapses by a GFP-based calibration technique. Nat Methods 2:677–684.
Takahashi RH, Almeida CG, Kearney PF, Yu F, Lin MT, Milner TA, Gouras GK (2004) Oligomerization of Alzheimer's β-amyloid within processes and synapses of cultured neurons and brain. J Neurosci 24:3592–3599.
Terry RD (2006) My own experience in early research on Alzheimer disease. J Alzheimers Dis 9 [Suppl 3]:117–119.
Trinczek B, Ebneth A, Mandelkow EM, Mandelkow E (1999) Tau regulates the attachment/detachment but not the speed of motors in microtubule-dependent transport of single vesicles and organelles. J Cell Sci 112:2355–2367.
Turner PR, O'Connor K, Tate WP, Abraham WC (2003) Roles of amyloid precursor protein and its fragments in regulating neural activity, plasticity and memory. Prog Neurobiol 70:1–32.
Wacker I, Kaether C, Kromer A, Migala A, Almers W, Gerdes HH (1997) Microtubule-dependent transport of secretory vesicles visualized in real time with a GFP-tagged secretory protein. J Cell Sci 110:1453–1463.
Walsh DM, Klyubin I, Fadeeva JV, Rowan MJ, Selkoe DJ (2002) Amyloid-beta oligomers: their production, toxicity and therapeutic inhibition. Biochem Soc Trans 30:552–557.
Walter J, Henke-Fahle S, Bonhoeffer F (1987) Avoidance of posterior tectal membranes by temporal retinal axons. Development 101:909–913.
Ward TH, Lippincott-Schwartz J (2006) The uses of green fluorescent protein in mammalian cells. Methods Biochem Anal 47:305–337.
Wilhelm S, Gröbler B, Gluch M, Heinz H (2003) Principles of confocal laser scanning microscopy, optical image formation, electronic signal processing. Jena, Germany: Zeiss.
Wittmann T, Waterman-Storer CM (2005) Spatial regulation of CLASP affinity for microtubules by Rac1 and GSK3beta in migrating epithelial cells. J Cell Biol [Erratum (2005) 171: 393] 169:929–939.
Yamazaki T, Selkoe DJ, Koo EH (1995) Trafficking of cell surface beta-amyloid precursor protein: retrograde and transcytotic transport in cultured neurons. J Cell Biol 129:431–442.